AJNR

MR Imaging of Cerebellopontine Angle and Internal Auditory Canal Lesions at 1.5 T

Gary A. Press and John R. Hesselink

AJNR Am J Neuroradiol 1988, 9 (2) 241-251
http://www.ajnr.org/content/9/2/241

MR Imaging of Cerebellopontine Angle and Internal Auditory Canal Lesions at 1.5 T

Gary A. Press[1]
John R. Hesselink

The high-field, thin-section (3–5 mm) MR imaging characteristics of 49 cerebellopontine angle and internal auditory canal lesions were reviewed. The diverse abnormalities include 20 acoustic neurinomas, eight neurinomas of other cranial nerves (six involving the fifth cranial nerve and two involving cranial nerves IX–XI), seven meningiomas, five subdural fluid collections, four brainstem tumors with exophytic components, three glomus jugulare tumors, one epidermoid tumor, and one basilar artery aneurysm. T1-, T2-, and proton-density-weighted images were obtained in all cases.

T1-weighted images most accurately showed the margins of the seventh and eighth nerves in the internal auditory canal and were most sensitive in detecting small tumors in the cerebellopontine angle. Differentiation of meningioma from acoustic neurinoma by MR was provided most reliably by separation of the meningioma from the porus acusticus and seventh and eighth nerves and not by signal-intensity differences. A hypointense vascular rim was noted on MR in seven of 13 extracanalicular acoustic tumors and in three of seven meningiomas.

Recent reports of MR imaging of the normal anatomy and of lesions of the cerebellopontine angle (CPA) and internal auditory canal (IAC) at low [1–5] and moderate [3, 6–8] magnetic field strengths have been most encouraging. Absence of beam-hardening artifacts, multiplanar imaging capability, and greater intrinsic soft-tissue contrast are emphasized as significant advantages of MR imaging relative to high-resolution CT in the assessment of tumors of the CPA and IAC. MR at 0.35 T was as accurate as gas CT in the diagnosis of all sizes of acoustic tumors [7]. The ability to demonstrate the normal contents of the IAC by MR facilitated differentiation of acoustic tumors from meningiomas and other lesions originating in the CPA [4, 7]. MR is now considered the diagnostic study of choice for the evaluation of patients with suspected acoustic neurinoma [3, 4, 9].

Prior reports of high-field-strength (1.5 T) MR of the CPA and IAC included only a few abnormal patients [10], described very small or intracanalicular tumors [11], or combined results of moderate (0.5 T) and high-field-strength imaging with 10-mm slice thickness [12]. We report the results of a large series of patients with diverse abnormalities of the CPA and IAC imaged exclusively at a high field strength with thin sections (3–5 mm).

Materials and Methods

We evaluated retrospectively 1000 consecutive brain MR examinations and identified 33 patients with 49 CPA and IAC lesions. Multiple lesions were found in five patients with known neurofibromatosis. One additional patient without neurofibromatosis had multiple lesions. The patients were 3–79 years old; 16 were females and 17 were males. The abnormalities included 20 acoustic neurinomas, eight additional cranial nerve tumors (six involving cranial nerve V and two involving cranial nerves IX–XI), seven meningiomas, five postoperative subdural fluid collections (three hematomas, two CSF hygromas), three glomus jugulare tumors, one epidermoid tumor, and one basilar artery aneurysm. Four patients with intraaxial

This article appears in the March/April 1988 issue of *AJNR* and the June 1988 issue of *AJR*.

Received July 9, 1987; accepted after revision October 6, 1987.

Presented at the annual meeting of the American Society of Neuroradiology, New York City, May 1987.

[1] Both authors: Department of Radiology and Magnetic Resonance Institute, University of California, San Diego, CA 92103-1990. Address reprint requests to G. A. Press, Department of Radiology, Box H–756, UCSD Medical Center, 225 Dickinson St., San Diego, CA 92103–1990.

***AJNR* 9:241–251, March/April 1988**
0195–6108/88/0902–0241

lesions that extended into the region of the CPA cistern were included also (one brainstem glioma and three ependymomas of the fourth ventricle).

Histologic proof was available for 20 lesions, angiographic verification in one lesion, and firm clinical and radiographic evidence in the others—12 acoustic neurinomas (nine in patients with neurofibromatosis), eight tumors involving cranial nerves other than the eighth nerve (all in patients with neurofibromatosis), five postoperative fluid collections, one meningioma, one brainstem glioma, and one glomus jugulare tumor.

MR was performed with a 1.5-T superconducting magnet.* In all cases, spin-echo pulse sequences were used: T2-weighted images had a repetition time (TR) of 1500–3000 msec and echo time (TE) of 70–80 msec and proton-density-weighted images had a TR of 1500–3000 msec and TE of 20 msec. Axial images were obtained in 31 patients, sagittal in four, and coronal in three. Slice thickness was 5 mm with a 2.5-mm interval between successive slices in all patients. A 256 × 256 matrix corresponding to a 0.75- by 0.75-mm pixel size was used in all examinations. T1-weighted images (TR = 600–800 msec, TE = 20 msec) were then obtained in all patients: coronal images in 21, axial in 18, and sagittal in 13. The slice thickness was 5 mm with a 2.5-mm interval between successive slices in the majority of cases. A 3-mm slice thickness with 1.5-mm gap was used in eight patients. In two instances, MR was repeated after IV administration of Gd-DTPA† at a dose of 0.1 mmol/kg. Pulse sequences after administration of Gd-DTPA were the same as for preenhancement MR studies.

The signal intensity of each lesion was described as hyperintense, isointense, or hypointense when compared with that of the adjacent upper pons on each image. We compared the ability of each of the three different MR images (T2-, proton-density-, and T1-weighted) to detect the lesion and to characterize it and its relationship to the basilar cisterns, brainstem, cerebellum, temporal bone, and vasculature at the base of the brain. For acoustic neurinomas each extracanalicular tumor component was measured in three dimensions: on axial images we recorded the largest diameter perpendicular (diameter A) and parallel (diameter B) to the posterior aspect of the petrous ridge; on coronal images, the largest superoinferior diameter (diameter C) was recorded.

In addition, the ability of MR to depict the normal anatomy of the unaffected IAC and CPA in patients with unilateral disease was assessed.

Results

Spin-echo sequences provided T2- and proton-density-weighted images with 5-mm section thickness in all 33 patients: axial images in 31 patients, sagittal in four, and coronal in three. These images demonstrated the IAC on both sides adequately in 23 patients and on one side in nine patients. Both IACs were seen poorly in only one subject.

At least one additional T1-weighted sequence was then performed in all 33 patients with special attention to the IACs. The large majority of the T1-weighted images were acquired in the coronal and axial planes. The IACs were adequately imaged on both sides in all subjects after this second sequence.

The T1-weighted sequence maximized the contrast between low-signal-intensity CSF and the seventh and eighth nerves, which were slightly hypo- or isointense relative to brain parenchyma (Fig. 1). This sequence often allowed the nerves to be seen from their origins at the surface of the pons to their terminations distally at the lateral aspect of the IAC.

On proton-density- and T2-weighted sequences, the CSF bathing the CPA and filling the IAC showed progressively higher signal intensity, obscuring the margins of the normally gracile nerve roots (Fig. 1).

Acoustic Neurinoma

A total of 20 acoustic tumors were imaged with MR (Table 1). Bilateral acoustic neurinomas were seen in five patients with neurofibromatosis. Unilateral lesions were seen in all other instances. Thirteen acoustic tumors had extra- and intracanalicular components. Seven lesions were completely intracanalicular. No lesion involved the extracanalicular portion of the eighth nerve exclusively. Fifteen lesions were newly diagnosed while five lesions were imaged after partial resection.

Of the 20 lesions detected, 19 were seen on unenhanced MR images; one additional lesion was demonstrated on MR only after IV administration of Gd-DTPA. The noncontrast T1-weighted images demonstrated 19 lesions, while noncontrast proton-density- and T2-weighted images detected 18 and 16 acoustic tumors, respectively. Small lesions were missed on unenhanced long TR (proton-density- and T2-weighted) images owing to increased signal intensity from CSF within the CPA and IAC causing obscuration of tumor margins (Fig. 1).

The smallest lesion detected on plain MR was an intracanalicular tumor measuring 3 × 7 mm. The lesion seen only by Gd-DTPA–aided MR was an even smaller intracanalicular tumor, measuring 3 × 3 mm. The largest acoustic tumor imaged measured 3.2 × 3.8 × 3.5 cm.

The large majority of acoustic neurinomas were hypointense on T1-weighted images and isointense on proton-density- and T2-weighted images.

Thirteen tumors were homogeneous in appearance on noncontrast MR. Three small intracanalicular tumors had heterogeneous signal intensity, likely from volume-averaging of surrounding CSF and temporal bone. Two of the largest tumors imaged were heterogeneous, possibly from necrosis. Heterogeneity in one additional moderate-sized lesion could be attributed confidently to calcification.

Plain MR images demonstrated erosion of the IAC in all 15 newly diagnosed tumors. Even the subtle canal asymmetry expected with small intracanalicular tumors was detected reliably. Axial MR sections were more useful than coronal images in demonstrating partial resection of the posterior wall of the IAC in the five postoperative cases.

All seven exclusively intracanalicular tumors caused obscuration of the seventh and eighth nerves and displacement of CSF from the IAC. These findings were best noted on T1-weighted images (Fig. 1).

Measurements of acoustic neurinomas revealed that extracanalicular components were not perfectly spherical; both diameter B and diameter C exceeded diameter A in eight of 13 cases. In general, the surface of the extracanalicular tumor component was smooth and convex toward the brainstem.

* Signa, General Electric, Milwaukee.
† Berlex, Cedar Knolls, NJ.

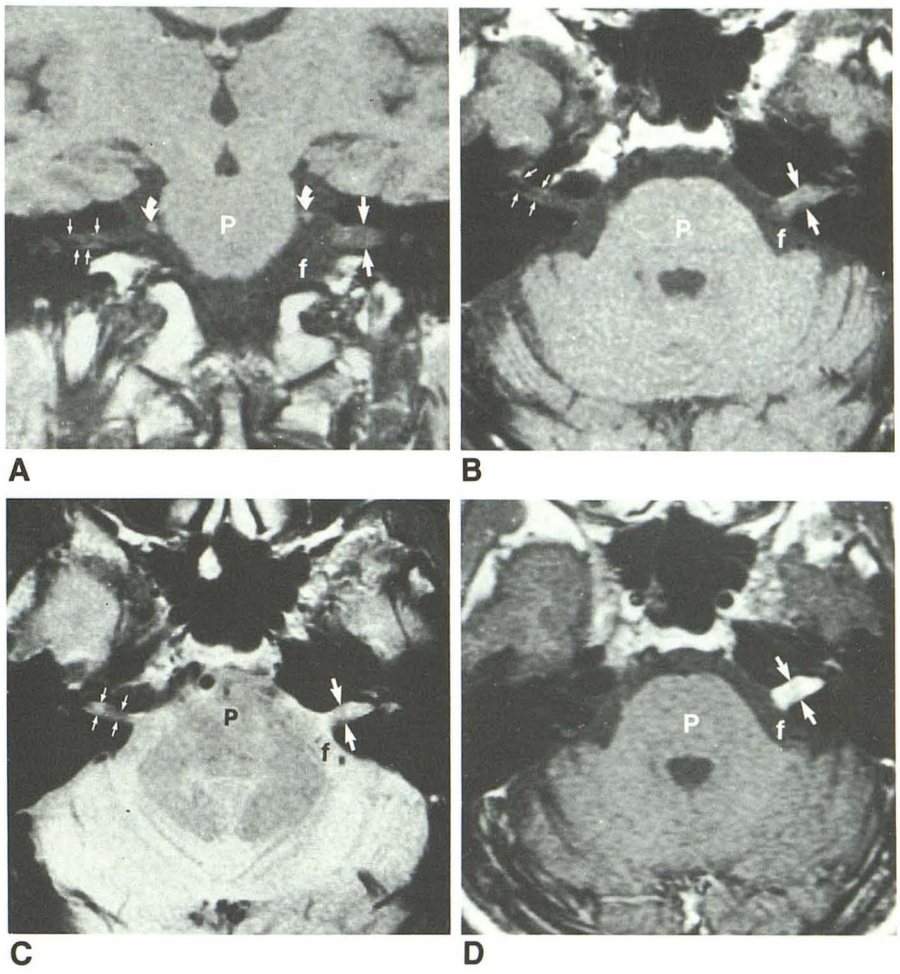

Fig. 1.—51-year-old man with intracanalicular acoustic neurinoma on left.

***A* and *B*, T1-weighted coronal (*A*) and axial (*B*) images show small internal auditory canal tumor (*large straight arrows*), slightly hypointense relative to normal pons (P), displacing lower-signal-intensity CSF (f) from enlarged left internal auditory canal. On normal right side, CSF occupies part of medial internal auditory canal, and normal seventh and eighth nerves may be distinguished further laterally (*small straight arrows*). Cisternal portions of both trigeminal nerves (*curved arrows*) are well seen in cross section, adjacent to pons on coronal image.**

***C*, Axial proton-density-weighted image. CSF has become brighter relative to brain parenchyma, thereby obscuring margins of seventh and eighth nerves on right side (small arrows) and small tumor in left internal auditory canal (*large arrows*).**

***D*, Axial T1-weighted image after IV Gd-DTPA shows homogenous enhancement of internal auditory canal tumor, increasing its conspicuity (compare with *B*).**

TABLE 1: Relative Signal Intensities of Cerebellopontine Angle and Internal Auditory Canal Masses

Type of Lesion	No. of Lesions											
	Total	T1				Proton Density				T2			
		Low	Iso	High	NS	Low	Iso	High	NS	Low	Iso	High	NS
Neoplastic:													
Acoustic neurinoma	20	16	3	0	1	0	14	4	2	0	12	4	4
Other neurinoma	8	6	2	0	0	0	8	0	0	0	8	0	0
Meningioma	7	4	3	0	0	1	1	5	0	1	1	3	2
Brainstem tumor	4	3	1	0	0	0	0	4	0	0	0	4	0
Glomus jugulare	3	2	1	0	0	0	2	1	0	0	1	2	0
Epidermoid	1	1	0	0	0	1	0	0	0	0	0	1	0
Subtotal	43	32	10	0	1	2	25	14	2	1	22	14	6
Nonneoplastic:													
Subdural fluid	5	2	0	3	0	2	0	3	0	0	0	5	0
Basilar aneurysm lumen	1	1	0	0	0	1	0	0	0	0	1	0	0
Subtotal	6	3	0	3	0	3	0	3	0	0	1	5	0
Total	49	35	10	3	1	5	25	17	2	1	23	19	6

Note.—MR sequences were T1-weighted (T1), proton-density-weighted (proton density), and T2-weighted (T2). Signal intensities were measured relative to that of the pons on the same unenhanced MR image. Low = less than; iso = equal to; high = greater than; NS = lesion not seen.

Displacement and/or compression of brainstem structures were well delineated by MR and noted in all seven tumors with extracanalicular extension of measured diameter A greater than 1.5 cm. Several discrete stages of impingement on the brainstem were noted. Initially, the ipsilateral lateral aspect of the pons and anterior portion of the middle cerebellar peduncle would be indented by the CPA mass. As the size of the mass increased, the entire brainstem including the midbrain and medulla would be shifted slightly to the contralateral side. The largest masses induced a distinctive rotation of the posterior aspect of the pons and brainstem away from the side of the neoplasm (Figs. 2 and 3).

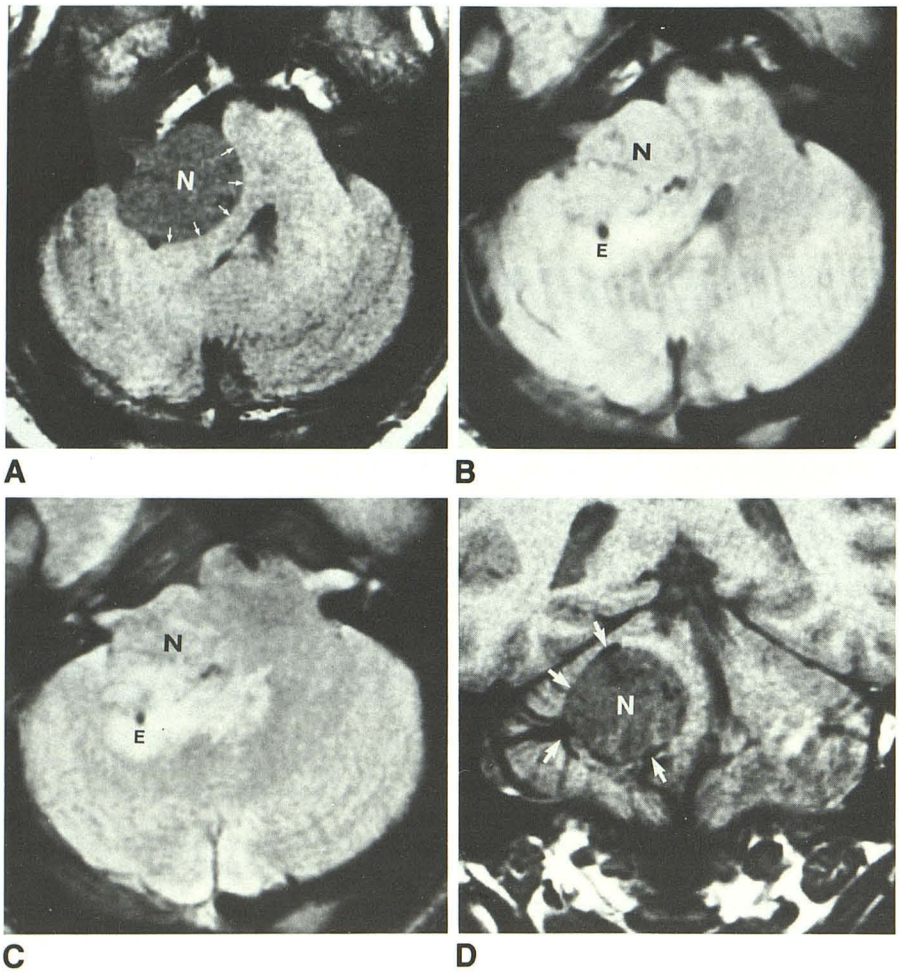

Fig. 2.—33-year-old man with 3- to 4-cm acoustic neurinoma.

***A*, Axial T1-weighted image. Lesion (N) is hypointense relative to normal pons. Compression of right middle cerebellar peduncle and rotation of posterior aspect of brainstem toward contralateral side (*arrows*) are well seen.**

***B* and *C*, Axial proton-density- (*B*) and T2- (*C*) weighted images. Lesion is isointense (*B*) and iso- to slightly hyperintense (*C*) relative to pons. Edema (E) within white matter of compressed peduncle has high signal intensity with long TR.**

***D*, Coronal T1-weighted image. Petrosal and capsular veins are displaced superiorly and inferiorly by mass, forming hypointense rim (*arrows*).**

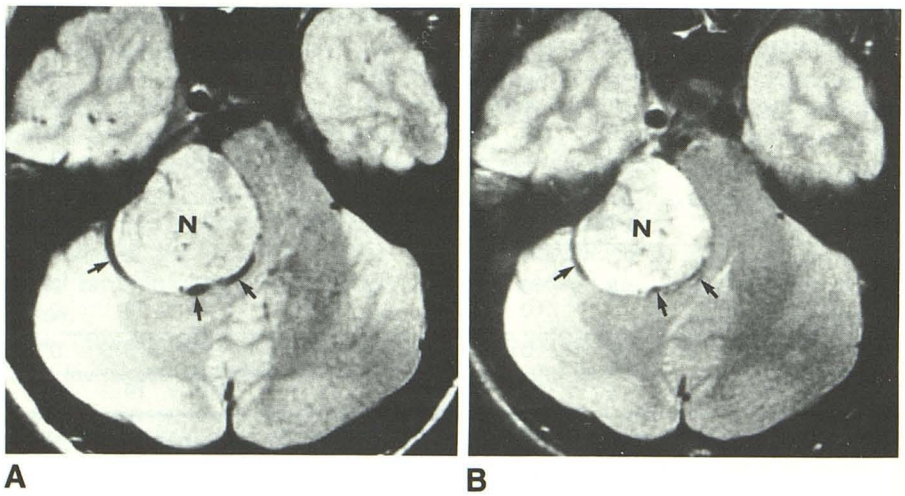

Fig. 3.—34-year-old woman with large acoustic neurinoma. Variability in signal-intensity characteristics of acoustic neurinomas is seen on proton-density- (*A*) and T2- (*B*) weighted images. Tumor (N) is hyperintense relative to normal pons (compare with Figs. 2B and 2C). Hypointense rim represents displaced tributaries of petrosal and capsular veins (*arrows*).

MR demonstrated displaced blood vessels at the periphery of seven of the 13 acoustic tumors with extracanalicular extension (Figs. 2 and 3). In six instances, the petrosal vein or its tributaries were noted to be deviated over the surface of the lesion. In one other case the posterior cerebral artery was deviated superiorly over the top of the mass. The presence of vascular displacement also seemed related to the size of the mass: six of eight tumors of diameter A equal to or greater than 1.4 cm were associated with this finding, while only one of five tumors less than 1.4 cm in diameter caused detectable vascular displacement. No similar "capsule" of displaced vessels was associated with the exclusively intracanalicular lesions.

Other Neurinomas

Eight tumors affecting cranial nerves other than the eighth nerve were detected in three patients with bilateral acoustic neurinomas and neurofibromatosis. Six tumors involved the fifth cranial nerve; two others involved cranial nerves IX–XI.

All six trigeminal neurinomas were 1 cm or less in size, isointense on T2- and proton-density-weighted images and isointense to hypointense on T1-weighted images relative to the adjacent pons (Table 1). All tumors were homogeneous in signal intensity.

Trigeminal neurinomas caused fusiform enlargement of the cisternal portion of the nerve in all cases (Fig. 4). In four instances the normal CSF signal within Meckel cave was completely replaced by signal intensity identical to that of tumor. Extension of neoplasm from the gasserian ganglion to involve the cisternal portion of the fifth nerve was diagnosed in those cases. In the two other tumors, the usual signal intensity of CSF filling Meckel cave was identified. No evidence of tumor within the superior ophthalmic fissure, foramen rotundum, or foramen ovale was seen in any of the trigeminal neurinomas.

On axial images it was sometimes difficult to define the margin between the cisternal fifth nerve tumor and the eighth nerve tumor lying immediately beneath and posterior to it. A coronal sequence was most helpful in each instance by showing the medial margin of the roof of the IAC separating the fifth nerve tumor above the petrous bone from the eighth nerve tumor within the IAC (Figs. 4 and 5).

The two jugular region neurinomas were less than 1 cm in size. Both were imaged within an expanded jugular foramen

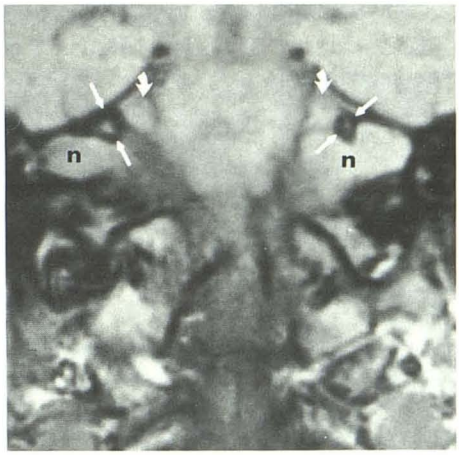

Fig. 5.—19-year-old man with neurofibromatosis. Coronal proton-density-weighted image distinguishes bilateral isointense fifth nerve tumors (*curved arrows*) above roofs of internal auditory canals (*straight arrows*) from bilateral eighth nerve tumors (n) within enlarged internal auditory canals. Acoustic tumor on left extends into cerebellopontine angle cistern.

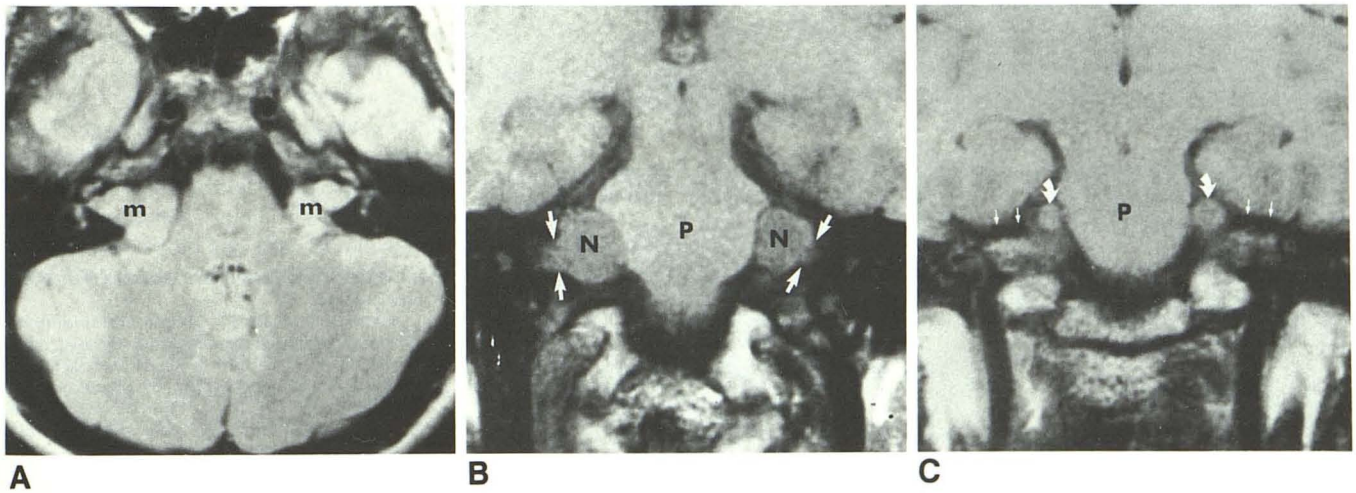

Fig. 4.—17-year-old girl with neurofibromatosis.

***A*, Axial proton-density-weighted image. Bilateral fifth and seventh nerve tumors are seen as single large masses (m) within both cerebellopontine angle cisterns.**

***B* and *C*, Coronal T1-weighted images distinguish hypointense (*B*) eighth nerve tumors (N) widening internal auditory canals (*large straight arrows*) and compressing pons (P) from isointense (*C*) neurinomas of cisternal portions of fifth nerves (*curved arrows*), cut in cross section above roofs of internal auditory canals (*small straight arrows*) on slightly more anterior section.**

and were associated with absence of the usual flow-related signal void on T1-, T2-, and proton-density-weighted images. The tumors appeared homogeneous and isointense relative to normal parenchyma on all sequences.

Meningiomas

Of seven meningiomas demonstrated by MR, two originated at the mouth of the IAC, and in one instance each at other locations: posterior aspect of the petrous ridge, free edge of the tentorium cerebelli, anterior aspect of the foramen magnum, superior aspect of the occipital bone, and within the jugular foramen. The size ranged from 1.5 to 4.0 cm in greatest diameter. All lesions were detected on T1- and proton-density-weighted images. The two smallest lesions were not observed on the T2-weighted images, likely secondary to volume-averaging of surrounding CSF within the CPA cistern (Fig. 6). The majority of meningiomas were hyperintense on T2- and proton-density-weighted images and hypointense on T1-weighted images (Table 1).

Four tumors were homogeneous in signal intensity on all pulse sequences. Three tumors were heterogeneous on at least one sequence. A vascular capsule or displacement of normal vessels about three lesions was well demonstrated by MR.

In several instances MR demonstrated important anatomic information that narrowed the differential diagnosis. In two patients with a mass at the orifice of the IAC, MR was able to image the entire course of the normal seventh and eighth nerves, thereby excluding acoustic neurinoma. In another patient, axial MR images demonstrated a mass in the region of the cisternal portion of the fifth nerve, possibly representing a neurinoma. Coronal MR images readily separated the mass from the course of the fifth nerve and showed the broad tentorial base of the lesion most consistent with a meningioma.

In one subject MR demonstrated tumor along the course of the maxillary and mandibular divisions of the fifth nerve as well as in the region of Meckel cave and in the prepontine cistern (Fig. 7). The appearance of this lesion mimicked that of trigeminal neurinomas as described previously, and fifth nerve tumor was the preferred MR diagnosis. At surgery, tumor was seen within the sheath investing the fifth nerve branches and invading the nerve itself; however, the final pathologic diagnosis was meningioma.

In one meningioma examined by both CT and MR, MR was

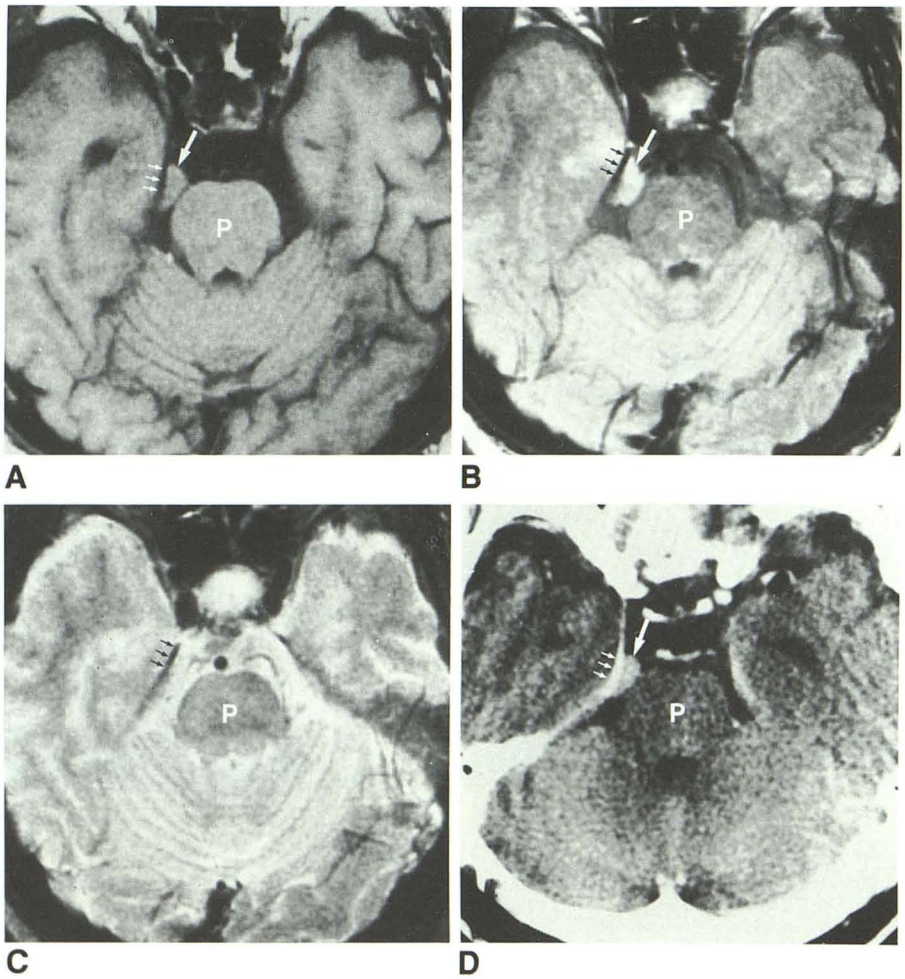

Fig. 6.—72-year-old man with 15-mm tentorial meningioma.

***A* and *B*, On axial T1- (*A*) and proton-density- (*B*) weighted images meningioma (*large arrows*), based on dura of right tentorial leaf (*small arrows*), is iso- (*A*) and hyper- (*B*) intense relative to normal pons (P). Tumor margins are well delineated from surrounding CSF, which has relatively low signal intensity.**

***C*, T2-weighted image at same level. Tumor no longer can be distinguished from surrounding high-signal-intensity CSF.**

***D*, Axial contrast-enhanced CT scan shows uniform enhancement of small mass lesion and thickening of adjacent tentorial leaf, suggesting tumor infiltration.**

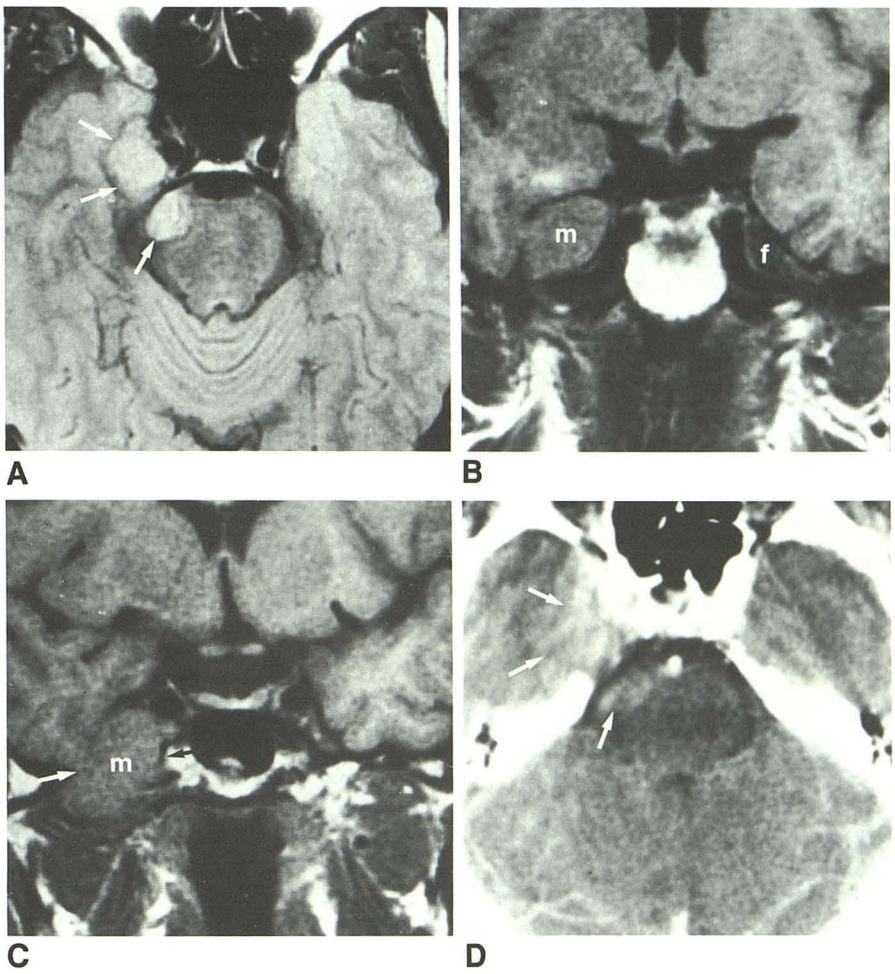

Fig. 7.—49-year-old woman with meningioma mimicking fifth nerve tumor.

***A*, Axial proton-density-weighted image shows oval lesion (*arrows*) following course of fifth nerve from prepontine cistern to region of Meckel cave on right. Mass is hyperintense relative to pons.**

***B*, Coronal T1-weighted image shows isointense mass (m) enlarging right Meckel cave. Low-signal CSF is preserved in normal-sized left Meckel cave (f).**

***C*, More anterior T1-weighted image shows lesion extending into infratemporal fossa through enlarged foramen ovale (*arrows*). On the basis of these MR findings, a diagnosis of trigeminal neurinoma was favored. At surgery, however, meningioma was found within sheath of fifth nerve and its branches.**

***D*, Contrast-enhanced axial CT image. Lesion (*arrows*) is partly obscured by beam-hardening artifacts at base of skull.**

considered inferior in accurately characterizing the lesion. This mass was demonstrated by CT to be a largely calcified tumor based on the dura overlying the right occipital bone. However, the MR appearance was particularly confusing. In the bed of the tumor MR demonstrated low signal intensity on T2-weighted images, which became relatively less hypointense on proton-density- and T1-weighted images (Fig. 8). The appearance resembled that of an acute hematoma, which could not be ruled out on the basis of MR alone.

Exophytic Brainstem Neoplasms

There were four brainstem tumors (three ependymomas and one glioma) with exophytic components extending into the region of the CPA cistern (Table 1). These tumors tended to be large, with axial diameters ranging from 3.4 to 5.9 cm. Each lesion in this group had regions of high signal intensity on both T2- and proton-density-weighted images and of iso- or hypointensity on T1-weighted images. Three lesions were heterogeneous in signal intensity on at least one pulse sequence.

The three ependymomas had similar morphologic characteristics on MR. In each case the lesion arose within the fourth ventricle and caused hydrocephalus. Tumor exited the fourth ventricle via one (two cases) or both (one case) foramina of Luschka to present to a variable degree within the CPA cistern (Fig. 9). Displacement of the medulla and pons away from the side of greatest CPA extension was seen in all cases. In two instances tumor extended downward through the foramen magnum and into the upper cervical spinal canal. Direct sagittal imaging was a great advantage of MR in depicting the intraventricular portion of these tumors and extension of the neoplasm into the spinal canal. In one case displacement of blood vessels around the margin of the lesion was demonstrated by MR.

The exophytic brainstem glioma expanded the right side of the medulla and pons and right cerebellar peduncle and extended directly into the CPA cistern (Fig. 10). The fourth ventricle was invaded by a small tongue of tissue. The vertebrobasilar junction was displaced slightly across the midline away from the side of tumor extension into the prepontine cistern.

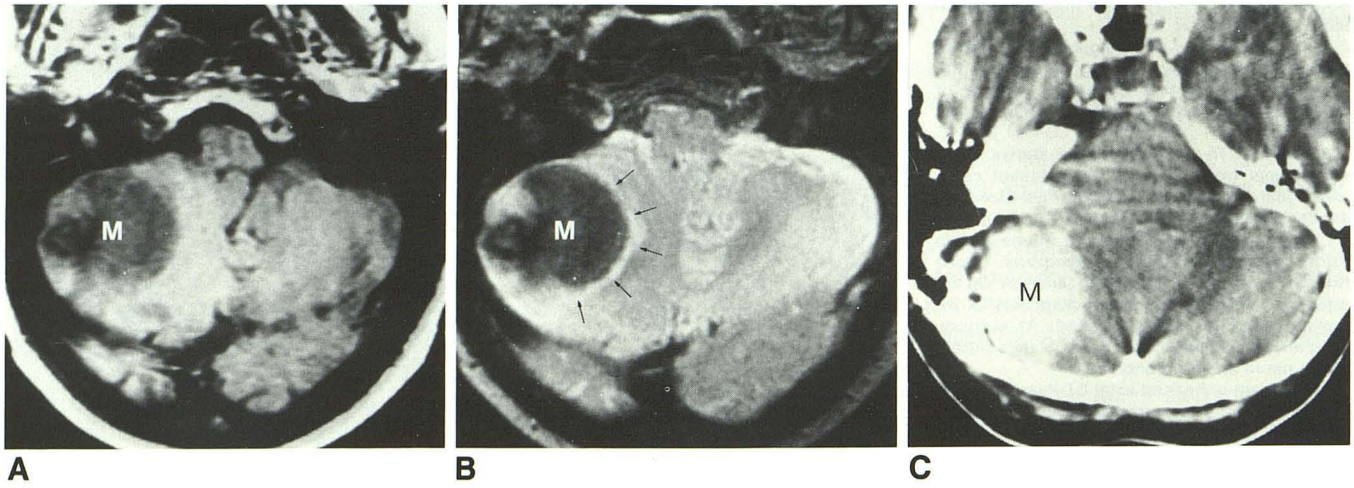

Fig. 8.—66-year-old woman with heavily calcified meningioma mimicking cerebellar hemorrhage.

***A*, Axial T1-weighted image. Round 4-cm lesion (M) within posterior fossa is hypointense.**

***B*, T2-weighted image. Lesion has become even more hypointense, suggesting acute hemorrhage within right cerebellar hemisphere. Thin rim of surrounding hyperintensity (*arrows*) represents parenchymal edema.**

***C*, On axial unenhanced CT scan, lesion density measures more than 150 H, consistent with calcification within large meningioma. Hyperostosis of occipital bone was noted on bone windows (not shown).**

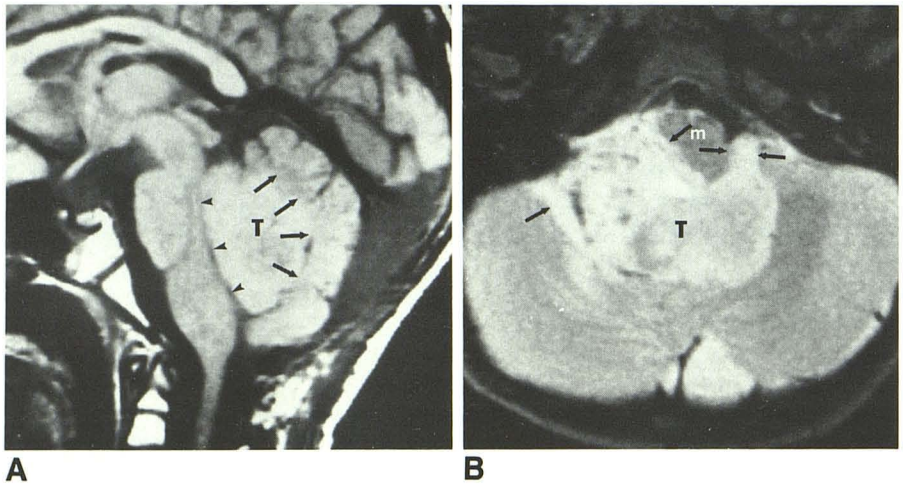

Fig. 9.—6-year-old girl with fourth ventricle ependymoma.

***A*, Sagittal T1-weighted image. Intraventricular origin of tumor (T) is seen particularly well. Mass displaces pons and medulla anteriorly (*arrowheads*), while vermis is displaced posteriorly (*arrows*).**

***B*, T2-weighted image. Hyperintense tumor exits fourth ventricle via widened foramina of Luschka (*arrows*). Medulla (m) is flattened against clivus and minimally shifted away from right side, the side of greatest cerebellopontine angle extension of tumor.**

Postoperative Fluid Collections

MR in five patients revealed postsurgical fluid collections of varying size extending into the CPA cistern (Table 1). In no instance was the fluid accumulation suspected before MR. In each instance the fluid was found on the same side as the prior surgical procedure. The collection appeared to lie within the subdural space in each case, since the inner aspect of the fluid conformed to the shape of the underlying cerebellum without dipping into the fissures while the outer aspect conformed to the inner table of the skull or undersurface of the tentorium cerebelli.

In two cases the signal intensity of the collection on all pulse sequences was homogeneous and similar to that of CSF, suggesting a diagnosis of subdural hygroma. In two other patients, the collection was homogeneous and hyperintense relative to brain parenchyma on all pulse sequences, compatible with subacute (>7 days) or chronic (>1 month) hematoma. The remaining patient, who had had a tentorial meningioma resected, had a collection that spanned the postoperative discontinuity in the tentorial leaf. The infratentorial component was compatible with subacute hematoma, as was a portion of the supratentorial component. The remainder of the supratentorial component had very low signal intensity similar to that of air on all pulse sequences.

The degree of mass effect varied with the size of the collection. The thinnest collection detected was 3 mm and caused modest effacement of fissures along the superior and anterior aspect of the cerebellar hemisphere. The larger collections (2–4 cm thick) caused displacement and/or compression of both the underlying brainstem and the middle cerebellar peduncle.

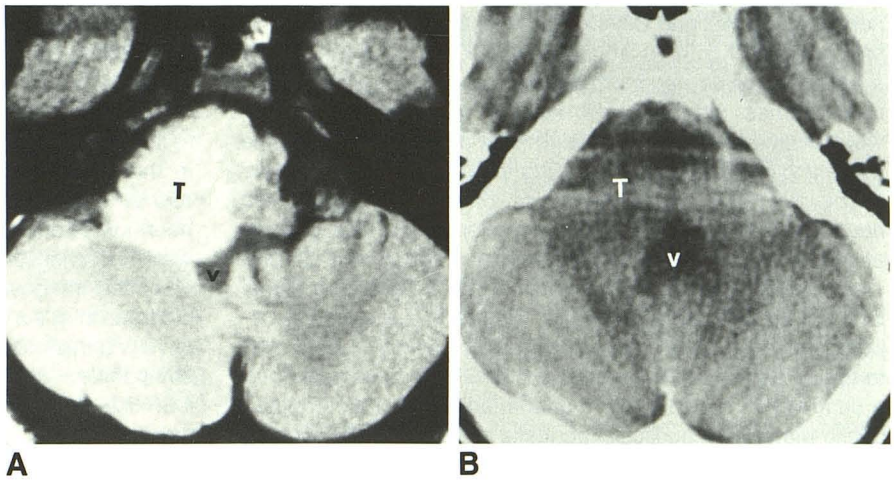

Fig. 10.—23-year-old man with brainstem glioma.

***A*, Axial proton-density-weighted image. Hyperintense tumor (T) expanding the right side of brainstem and invading fourth ventricle (v) is well seen.**

***B*, Contrast-enhanced CT scan. Slightly hypointense tumor is less apparent owing to interpetrous beam-hardening artifacts.**

In one case MR was superior to contrast-enhanced CT in characterizing a chronic subdural hematoma. In this patient, CT demonstrated a peripheral low-density region incorrectly interpreted as encephalomalacia of the lateral aspect of the right cerebellar hemisphere. No enhancing membrane was present. Subsequent MR showed the true extraaxial location of the lesion and its high signal intensity on T1-weighted images characteristic of chronic hemorrhage.

Miscellaneous Tumors

The three glomus jugulare tumors, two with histologic proof and one presumed on clinical grounds, completely replaced the usual jugular bulb flow-void with slightly hypo- to hyperintense signal on all image sequences in all planes (Table 1). No evidence was seen of even-echo rephasing phenomena or high-velocity signal loss. In one patient, sheetlike tumor lined the posteroinferior aspect of the petrous ridge above the jugular foramen, and was in continuity with a more rounded mass extending inferiorly from the foramen into the neck. The other two lesions were more circumscribed and occupied the region between the distal end of the sigmoid sinus and the inferior aspect of the jugular foramen. Tumors tended to be iso- to hyperintense on proton-density- and T2-weighted images and hypointense on T1-weighted images. Two tumors were homogeneous on all images while the remaining lesion was heterogeneous.

One proven epidermoid was imaged with MR before surgical resection (Table 1). The mass extended as a sheet within the left CPA cistern from the level of the medulla to the level of the midbrain. The signal intensity of the lesion was hyperintense relative to that of the pons on T2-weighted images, slightly hypointense on proton-density-weighted images, and hypointense on T1-weighted images. Overall its signal intensity was similar to that of normal CSF, and a diagnosis of arachnoid cyst was also entertained preoperatively. The basilar artery was displaced to the right of the midline by the large mass.

Basilar Aneurysm

Absent signal owing to flowing blood was shown by MR in the patent lumen of a partially thrombosed fusiform basilar artery aneurysm on sagittal T2-, proton-density-, and T1-weighted images (Table 1). In the region of intraluminal thrombus, mixed hyperintense and slightly hypointense signal was demonstrated on all pulse sequences. These MR findings provided diagnostic specificity in this case. The aneurysm measured 2 cm in cross-sectional diameter and caused compression of the pons.

Discussion

Prior studies of the CPA and IAC have found different MR pulse sequence parameters to be indicated for imaging the cisternal or intracanalicular portions of the seventh and eighth nerve complex. At 0.6T, the best visualization of the acoustic nerves in their intracanalicular portion was obtained by using spin-echo images with TR = 1500 msec, TE = 60 msec, while TR = 500 msec, TE = 30 msec was best for the cisternal portion [9]. All images in that study were obtained with 8-mm slice thicknesses. At 1.4–1.5 T, definition of the acoustic nerves and tumors seemed better in 3- or 5-mm-thick sections than in 10-mm sections with a smaller number of averages [10]. Heavily T1-weighted partial saturation images demonstrated the seventh and eighth cranial nerves better than spin-echo images did, in which CSF had a higher signal intensity than parenchyma [10].

Theoretical calculations of relative resolving power were used to determine the best sequence for detecting small tumors in the CPA and IAC at 1.5 T [13]. The authors emphasized that CSF bathes small lesions in the CPA as well as the seventh and eighth nerves in the IAC. To detect the smallest CPA and IAC lesions, the border between tumor or nerve and CSF must be shown accurately [13]. A TR of 800 msec was best from theoretical calculations and proved best in control and tumor patients [13]. Our results confirm that the margin between CSF and normal seventh and eighth

nerves in the IAC and CPA is best delineated by the short TR sequence at 1.5 T; in addition, in our series, three of the smallest acoustic neurinomas and two of the smallest CPA meningiomas, although well seen on T1-weighted images, were missed on heavily T2-weighted images owing to volume averaging of bright CSF obscuring the margins of the tumor.

The plain MR characteristics of intracanalicular acoustic neurinomas in our series include erosion of the IAC, obscuration of the margins of the seventh and eighth nerves, and displacement of CSF from the canal. Heterogeneous signal intensity of three intracanalicular tumors in our series is believed to result from volume averaging of normal CSF and temporal bone surrounding the lesion. Others have described a central thin band of low signal intensity of undetermined cause within intracanalicular acoustic tumors [11]. This finding was not seen in our series. The utility of Gd-DTPA–enhanced MR imaging in the investigation of postoperative recurrence of acoustic neurinomas has been reported [14]. In our series, one recurrent/residual intracanalicular lesion missed on plain MR was detected after IV administration of Gd-DTPA.

All extracanalicular acoustic tumor components were centered at the porus acusticus. The majority were hypointense on T1-weighted images and isointense on T2- and proton-density-weighted images. Heterogeneity was seen in several lesions and possibly was from necrosis. Calcification was detected by MR in one lesion. Compression of the middle cerebellar peduncle and brainstem always resulted when the extracanalicular mass measured more than 1.5 cm in transverse diameter. The largest lesions caused a distinctive rotation of the posterior aspect of the brainstem away from the affected side. A vascular capsule was noted surrounding 54% of extracanalicular components in our series. The capsule appeared as a rim of low signal intensity on all images. Extracanalicular lesions with transverse diameters of 1.4 cm or larger were more likely to have such a capsule. The capsule most commonly represented petrosal veins displaced from the posterior aspect of the petrous ridge by the expanding mass lesion. To our knowledge, this represents the first description of the MR appearance of a vascular rim surrounding extracanalicular acoustic neurinomas. Findings reported in an earlier angiographic study are strikingly similar to ours [15]. In that report, posterior and lateral displacement of the petrosal veins and their tributaries were noted in 22 of 30 acoustic neurinomas. Lesions less than 1.5 cm in greatest diameter did not show any vascular displacement [15]. In a previous MR study similar hypointense rim was reported in 66% of 32 primarily supratentorial meningiomas [16].

The MR appearance of the normal trigeminal nerve and its branches was recently described and correlated with cryomicrotomic sections [17]. Only a few descriptions of the MR appearance of unilateral trigeminal neurinomas are available [17, 18]; there has been no previous description of bilateral trigeminal neurinomas. In one report [17], a unilateral solid tumor involving only the trigeminal ganglion replaced the low-intensity signal from Meckel cave with signal similar to that of brain tissue on T1-weighted images. In another report, a cystic neurinoma appeared as a smoothly marginated mass that was hypointense relative to normal parenchyma on T1-weighted images and hyperintense on T2- and proton-density-weighted images [18]. The mass extended from the prepontine cistern into Meckel cave and emerged in the cavernous sinus.

In our series, trigeminal neurinomas were noted bilaterally in three pateints with neurofibromatosis. Each patient also had simultaneous bilateral eighth nerve tumors. All trigeminal neurinomas appeared solid, being slightly hypointense on T1-weighted images and isointense on proton-density- and T2-weighted images. The cisternal segment of the nerve was enlarged in all six tumors, and the CSF-like signal from Meckel cave was replaced by signal similar to brain in four instances, compatible with involvement of the ganglion as well. Normal CSF-like signal emanated from Meckel cave in the two remaining tumors, implying that only the cisternal portion of the nerve was involved with sparing of the trigeminal ganglion. Early anatomic studies [19–21] revealed that the most common site of origin of trigeminal neurinomas seems to be at a point *between* the ganglion and the nerve root itself; in one series, 32 trigeminal neurinomas were divided morphologically into three groups: (1) involving predominantly the gasserian ganglion (47%), (2) involving predominantly the nerve root (34%), and (3) involving both ganglion and root equally (19%) [21]. Included in our series is the first MR description of trigeminal neurinoma involving predominantly the nerve root within the posterior fossa.

Prior studies reporting the MR appearance of infratentorial meningiomas have emphasized their variable signal intensity, especially on T2-weighted images [4, 12]. In our series, the majority of meningiomas were hyperintense relative to the pons on both T2- and proton-density-weighted images. Acoustic neurinomas were more often isointense relative to the pons on long TR images than meningiomas were; however, there was overlap between the signal intensities of the two tumors. Differentiation of meningiomas from acoustic neurinomas in our series depended on separation of the meningioma from the IAC in five instances and visualization of the normal seventh and eighth nerves in the two instances in which a lesion was present at the mouth of the porus acusticus. Displacement of vessels around the periphery of the mass was noted in several instances, as described previously [4, 12]. Two meningiomas in our series had particularly unusual appearances on MR. In one case, a lesion affecting the trigeminal nerve sheath mimicked the appearance of a neurinoma; in the other case, a large, heavily calcified meningioma was hypointense on T2- and T1-weighted images, reminiscent of an acute hemorrhage.

MR was most helpful in establishing the true intraaxial origin of exophytic brainstem neoplasm and fourth ventricular tumors in our series. Such extension of intraaxial neoplasm into the CPA is common, occurring in 55% of all posterior fossa ependymomas and 60% of all brainstem gliomas at gross pathology [22]. The extension of fourth ventricular ependymoma laterally into the CPA via the foramen of Luschka and/or inferiorly into the cervical spinal canal via the foramen magnum was shown by MR. Brainstem glioma was noted to extend directly into the CPA from its origin in the pons. T1 and T2 were prolonged in all cases.

Clinically unsuspected subdural fluid collections within the CPA were clearly recognizable with MR by their characteristic morphology and mass effect. CSF-like fluid, subacute (>7 days) or chronic (>1 month) blood, and mixed blood and air collections were readily distinguished by their different MR signal intensities.

In summary, the ability of MR to depict the entire course of the seventh and eighth nerves without artifacts on T1-weighted images was advantageous in differentiating acoustic neurinoma from meningioma at the porus acusticus. Displaced vessels forming a hypointense rim around acoustic neurinomas and meningiomas were demonstrated well by MR; such vessels may be obscured by adjacent enhancing tumor tissue on contrast-enhanced CT. Direct coronal MR images were helpful in separating bilateral trigeminal neurinomas from bilateral acoustic schwannomas in patients with neurofibromatosis. Chronic subdural hematoma mimicking peripheral cerebellar encephalomalacia on CT was recognized as an extraaxial high-signal-intensity fluid collection on MR images. The direct sagittal imaging capability of MR was useful in determining the site of origin of exophytic intraaxial lesions and the amount and route of tumor extension into the CPA and upper cervical canal. MR allowed the confident diagnosis or exclusion of a vascular cause for masses in the vicinity of the trigeminal portion of the carotid artery, basilar artery, or jugular bulb, as demonstrated in several instances of trigeminal neurinoma, basilar aneurysm, and glomus jugulare.

The failure of MR to demonstrate calcification definitively caused diagnostic uncertainty only in one instance of a large meningioma appearing as a region of hypointensity on all images reminiscent of an acute hematoma. A more specific diagnosis was obtained by CT in this case.

REFERENCES

1. Davidson HD, Ouchi T, Steiner RE. NMR imaging of congenital intracranial germinal layer neoplasms. *Neuroradiology* **1985**;27:301–303
2. Randell CP, Collins AG, Young IR, et al. Nuclear magnetic resonance imaging of posterior fossa tumors. *AJR* **1983**;141:489–496
3. Kingsley DPE, Brooks GB, Leung AWL, Johnson MA. Acoustic neuromas: evaluation by magnetic resonance imaging. *AJNR* **1985**;6:1–5
4. Mikhael MA, Ciric IS, Wolff AP. Differentiation of cerebellopontine angle neuromas and meningiomas with MR imaging. *J Comput Assist Tomogr* **1985**;9:852–856
5. Young IR, Bydder GM, Hall AS, et al. The role of NMR imaging in the diagnosis and management of acoustic neuroma. *AJNR* **1983**;4:223–224
6. Maslan MJ, Latack JT, Kemink JL, Graham MD. Magnetic resonance imaging of temporal bone and cerebellopontine angle lesions. *Arch Otolaryngol Head Neck Surg* **1986**;112:410–415
7. House JW, Waluch V, Jackler RK. Magnetic resonance imaging in acoustic neuroma diagnosis. *Ann Otol Rhinol Laryngol* **1986**;95:16–20
8. Lee BCP, Kneeland JB, Deck MDF, Cahill PT. Posterior fossa lesions: magnetic resonance imaging. *Radiology* **1984**;153:137–143
9. New PFJ, Bachow TB, Wismar GL, Rosen BR, Brady TJ. MR imaging of the acoustic nerves and small acoustic neuromas at 0.6 T: prospective study. *AJNR* **1985**;6:165–170
10. Daniels DL, Herfkins R, Koehler PR, et al. Magnetic resonance imaging of the internal auditory canal. *Radiology* **1984**;151:105–108
11. Daniels DL, Millen SJ, Meyer GA, et al. MR detection of tumor in the internal auditory canal. *AJNR* **1987**;8:249–252
12. Gentry LR, Jacoby CG, Turski PA, et al. Cerebellopontine angle–petromastoid mass lesions: comparative study of diagnosis with MR imaging and CT. *Radiology* **1987**;162:513–520
13. Enzmann DR, O'Donohue J. Optimizing MR imaging for detecting small tumors in the cerebellopontine angle and internal auditory canal. *AJNR* **1987**;8:99–106
14. Curati WL, Graif M, Kingsley DPE, Niendorf HP, Young IR. Acoustic neuromas: Gd-DTPA enhancement in MR imaging. *Radiology* **1986**;158:447–451
15. Takahashi M, Okudera T, Tomanaga M, Kitamura K. Angiographic diagnosis of acoustic neurinomas: analysis of 30 lesions. *Neuroradiology* **1971**;2:191–200
16. Zimmerman RD, Fleming CA, Saint-Louis LA, et al. Magnetic resonance imaging of meningiomas. *AJNR* **1985**;6:149–157
17. Daniels DL, Pech P, Pojunas KW, et al. Trigeminal nerve: anatomic correlation with MR imaging. *Radiology* **1986**;159:577–583
18. Brant-Zawadzki M, Kelly W. Brain tumors. In: Brant-Zawadzki M, Norman D, eds. *Magnetic resonance imaging of the central nervous system*. New York City: Raven, **1987**:151–185
19. Olive I, Svien HJ. Neurofibromas of the fifth cranial nerve. *J Neurosurg* **1957**;14:484–503
20. Schisano G, Olivecrona H. Neurinomas of the gasserian ganglion and trigeminal root. *J Neurosurg* **1960**;17:306–322
21. Jefferson G. The trigeminal neurinomas with some remarks on malignant invasion of the gasserian ganglion. In: *Proceedings of the Congress of Neurological Surgeons*, vol. 1. **1955**:11–54
22. Naidich TP, Zimmerman RA. Primary brain tumors in children. *Semin Roentgenol* **1984**;19:100–114